X-ray induced dynamics in borate glasses with different network connectivity

G. Pintori,[1,*] G. Baldi,[1] F. Dallari,[2] A. Martinelli,[1] M. Sprung,[2] and G. Monaco[1,†]
[1]*Department of Physics, University of Trento, Povo, Trento I-38123, Italy*
[2]*Deutsches Elektronen-Synchrotron DESY, Notkestraße 85, 22607 Hamburg, Germany*

(Received 26 February 2021; accepted 15 March 2022; published 28 March 2022)

Hard x rays induce atomic dynamics in oxide glasses at doses low enough that the average structure is unchanged. X-ray photon correlation spectroscopy is used here to study this effect in a series of alkali borate glasses characterized by different network connectivity. The product of the x-ray dose rate per atom and the decay time of the density correlation function is a sample-dependent parameter with the dimensions of an energy: It varies between a fraction of eV and few tens of eV and is sensitive to the network connectivity of the glass. It can then be used to access some bonding information also in cases where the x rays perturb the material, a regime of great interest in modern x-ray-based experiments.

DOI: 10.1103/PhysRevB.105.104207

I. INTRODUCTION

Since their first detection in 1895, x rays have been used for many fundamental discoveries and remarkable applications, playing a crucial role in solid state physics and medical diagnostics [1]. One of the main reasons for this success lies in the fact that the x-ray wavelength is comparable to the interatomic distance: a number of techniques originally developed using visible light has then been adapted to the x-ray range in order to achieve microscopic resolution. One such example is x-ray photon correlation spectroscopy (XPCS) [2], the x-ray version of the well-known dynamic light scattering [3]. XPCS is used to probe the spontaneous atomic dynamics in condensed matter at the atomic length scale [2,4–6], and for this reason increasing attention has been directed to it.

Despite the fact that the x-ray–matter interaction is a well established topic overall, the high brilliance provided by synchrotron radiation and x-ray free electron lasers is giving rise to complex and somewhat unexpected effects [7,8]. One example is the focus here: XPCS experiments have shown that an atomic motion is induced at temperatures well below the glass transition when shining an x-ray beam on an oxide glass [9–13]. The induced motion is present already at relatively low doses, when the average structure remains unaffected. This effect has a peculiar signature: its characteristic timescale, i.e., the time required for a complete renewal of the atomic configuration (the set of initial atomic positions), is inversely proportional to the x-ray dose rate. As a consequence, an oxide glass—a system frozen in an out-of-equilibrium configuration—changes completely its configuration in a matter of seconds when exposed to the x-ray dose rates typically available at synchrotron radiation sources. The trigger of this x-ray induced dynamics has been attributed to radiolysis [9,14,15].

This peculiar x-ray induced effect is here studied carrying out a systematic XPCS investigation on the series of alkali borate glasses $(M_2O)_x(B_2O_3)_{1-x}$, where M = Li, Na, and K and x is the metal oxide molar fraction. Pure boron oxide (B_2O_3) glass is made of a network of trigonal BO_3 groups [16–19]. The addition of an alkali-metal oxide to B_2O_3 up to about $x = 0.3$ causes a progressive increase of the number of four-coordinated boron units at the expense of the three-coordinated ones; the further addition of alkali-metal oxide up to about $x = 0.5$ causes the depolymerization of the glassy network via the creation of terminal, nonbridging oxygens [16,17,20]. The series of alkali borate glasses then offers an interesting playground to change independently network connectivity and chemical composition which puts it at the focus of both curiosity-driven research and technological applications [21]. Specifically, when varying the network modifier group M_2O at a fixed molar fraction x, these glasses are characterized by the same network connectivity [20] but by a different chemical composition; when changing instead the molar fraction for a given alkali modifier, it is possible to investigate the role played by the network connectivity on the glass properties. Exploiting this tunability, we show here that the x-ray induced dynamics depends only on the x-ray dose rate and on the connectivity of the glass network: for a given dose rate, the induced dynamics is faster the higher the network connectivity. One exception to this trend is also encountered and a possible reason for this is discussed.

II. EXPERIMENT

Glasses of composition $(M_2O)_x(B_2O_3)_{1-x}$ with M = Li, Na, and K were prepared using reagent-grade alkali carbonate and 99%-purity B_2O_3 powder purchased from Sigma-Aldrich. These materials were all heated up to 423 K and kept there for 16 h to reduce the water content. For what concerns the alkali borate glasses, appropriate amounts of B_2O_3 and M_2O dehydrated powders were melted in an alumina crucible at

*giovanna.pintori@unive.it
†giulio.monaco@unipd.it

TABLE I. List of some relevant parameters for the glasses studied here. The different alkali borate glasses of formula $(M_2O)_x(B_2O_3)_{1-x}$ are labeled with MBO and x, where M = Li, Na, or K and x is the metal oxide molar fraction. The glass transition temperature T_g is from Ref. [22]; the mass density, ρ, from Refs. [23,24]; L is the thickness of the samples used for the experiments discussed here, calculated from the measured x-ray transmission of the sample $T = \exp[-\mu L]$, with μ the attenuation coefficient; β is the shape parameter of the autocorrelation functions, a fitted parameter; and $\langle E_a(Q_{\max})\rangle$ has been calculated using Eq. (3).

Sample label	x	T_g [22] (K)	ρ [23,24] (g/cm^3)	L (μm)	β	$\langle E_a(Q_{\max})\rangle$ (eV)
LiBO	0	526	1.81	50±2	0.84 ± 0.03	0.73 ± 0.03
NaBO	0.14	660	2.10	66±1	0.93 ± 0.03	2.9±0.1
KBO	0.14	633	2.08	48±9	0.84 ± 0.04	2.8±0.1
LiBO	0.14	672	2.01	81±3	0.99 ± 0.06	2.7±0.1
LiBO	0.22	759	2.15	78±2	0.9±0.2	4.9±0.6
LiBO	0.30	767	2.24	113±3	0.91 ± 0.07	6.8±0.4
LiBO	0.50	663	2.18	54±3	0.75 ± 0.05	16±1

1300 K and kept there for 2 h, with M = Na and K at the composition $x = 0.14$, and M = Li at the compositions $x = 0.14, 0.22, 0.30$, and 0.50. The melts were then directly poured onto a mold preheated at 470 K, obtaining cylinders of 10 mm in diameter and 3 cm in height. For what concerns the pure B_2O_3 glass, the dehydrated powder was melted as well in an alumina crucible and a clear bubble-free melt was obtained after 24 h at 1230 K. The melt was then quickly cooled to room temperature pressing it between two metallic plates to produce a glass. All glasses were annealed for 6 h at about 20 K below their glass transition temperature. The glasses were cut with diamond tools into disks of about ∼2 mm in height and then polished to achieve a thickness of 50–100 μm. Since these glasses are hygroscopic, the polishing was done using ethanol, and subsequently they were kept under vacuum as much as possible and gently polished one more time just before the measurements in order to eliminate the surface exposed to atmospheric humidity. The final thickness was chosen as a compromise between optimizing the scattered intensity and keeping a reasonably good contrast [2]. The thickness of the studied samples is reported in Table I together with other useful parameters.

The XPCS experiment was performed at the beamline P10 of the PETRA III storage ring in Hamburg, Germany [25]. The x-ray beam of energy $E_{\rm ph} = 8.4$ keV was monochromatized using a Si(111) channel cut, and its spatially coherent part was focused onto a 3×3 μm^2 spot (FWHM) at the sample stage. The alkali borate glass samples were mounted in a vacuum chamber with kapton windows. The x-ray intensity, $I(Q,t)$, scattered in the horizontal plane at a given scattering angle θ and time t was measured in transmission geometry using a Princeton charge-coupled device (1340 × 1300 pixels, 20×20 μm^2 pixel size) placed ∼40 cm downstream from the sample. Here $Q = (4\pi/\lambda)\sin(\theta/2)$ is the scattering vector and λ is the x-ray beam wavelength [2]. The detector was in air, and a fly path in vacuum with kapton windows was installed between the sample chamber and the detector. The XPCS measurements were performed at room temperature and at the scattering vector, $Q_{\max}$, corresponding, for each sample, to the maximum of the structure factor. For each sample, several measurements were carried out with different incident beam fluxes, F, selected by means of absorbers. The reproducibility of the results was checked by repeating the measurements at different sample positions.

For each measurement, the dose rate per atom was calculated as $d = E_{\rm ph}\langle F\rangle_{\rm abs}/N_{\rm tot}$. Here, $\langle F\rangle_{\rm abs} = \langle F\rangle[1 - \exp(-\mu L)]$ is the absorbed x-ray flux, with μ the absorption coefficient of the material and L the sample thickness; $\langle F\rangle = F\,\Delta t_e/\Delta t_l$ is the average x-ray flux, where Δt_e is the exposure time, $\Delta t_l = \Delta t_e + \Delta t_r$ is the time in between two images, and $\Delta t_r = 2.2$ s the detector readout time; and $N_{\rm tot}$ is the number of atoms in the scattering volume, assuming an elliptical cross section for the beam with major and minor semiaxes equal, along the horizontal and vertical directions, to the corresponding FWHM/$\sqrt{2\ln(2)}$ values.

Information on the microscopic dynamics of the samples was obtained by calculating the normalized correlation function of the scattered intensity by the multispeckle method [26,27] to obtain a set of temporal correlation functions:

$$g_2(Q,t) = \langle I(Q,0)I(Q,t)\rangle/\langle I(Q,t)\rangle^2, \tag{1}$$

where the average $\langle\cdots\rangle$ is performed on both the detector pixels and the time series. The $g_2(Q,t)$ functions were modeled by the Kohlrausch-Williams-Watts (KWW) stretched exponential ansatz [28]:

$$g_2(Q,t) = 1 + \mathcal{C}(Q)\exp\{-2[t/\tau(Q)]^{\beta(Q)}\}, \tag{2}$$

where $\mathcal{C}(Q)$ is the contrast, $\beta(Q)$ defines the shape of the correlation function, and $\tau(Q)$ is the characteristic decay time of the Q component of the density fluctuations [2,3].

The effects of sample damage under x-ray illumination were carefully checked monitoring the Q dependence of the scattered intensity, $I(Q)$. Up to a total absorbed dose of about 1.1 GGy negligible changes in the average structure were observed. This is shown, for example, in Fig. 1, where the $I(Q)$ data measured for $(Li_2O)_{0.5}(B_2O_3)_{0.5}$ are reported for different accumulated doses during the acquisition of an XPCS scan. As can be seen, up to a total dose of 1.1 GGy of the scattered intensity is stable within 2% accuracy, though a more careful analysis reveals that it decreases continuously with increasing the dose. All the time series used to compute the autocorrelation functions $g_2(Q,t)$ reported here correspond to a total absorbed dose below 1.1 GGy.

The shortest utilized acquisition time was $\Delta t_e = 0.2$ s, the limit given by the counting statistics. While the datasets cor-

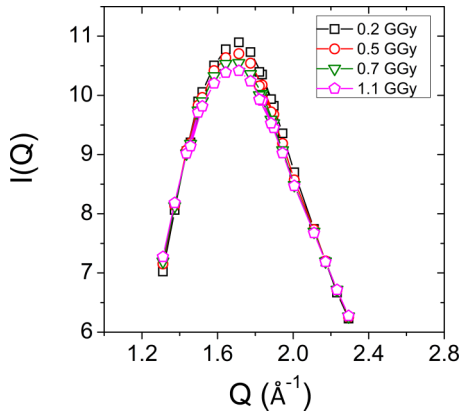

FIG. 1. Total scattered intensity profile measured in $(Li_2O)_{0.5}(B_2O_3)_{0.5}$ for different doses, as specified in the legend. The data are normalized by the incoming beam intensity after background subtraction.

responding to lower dose rates show a slow enough dynamics (on the timescale of Δt_e) that allows fitting Eq. (2) leaving all three parameters free [$\mathcal{C}(\mathcal{Q})$, $\tau(Q)$, $\beta(Q)$], this is not possible for curves collected for high enough dose rates where the decay time is fast and the curves are not complete. It can, however, be reasonably assumed that the parameter $\mathcal{C}(\mathcal{Q})$ is independent of the used absorber and is thus a constant for each sample. In the cases where it was possible to extract $\mathcal{C}(\mathcal{Q})$ from correlation functions measured for different incident beam fluxes or, rather, different dose rates per atom, this was indeed the case, as shown in the example of Fig. 2. The fits of Eq. (2) to the experimental curves corresponding to different x-ray dose rates were then carried out using a single contrast value. Specifically, for each sample, the XPCS curve(s) with a characteristic time sufficiently long to allow describing them with Eq. (2) leaving all parameters free were fitted first; the obtained value of the contrast was then fixed when modeling the XPCS curves for the same sample corresponding to different (higher) x-ray dose rates. It is worth underscoring that the obtained values of $\mathcal{C}(\mathcal{Q})$ are always small, of the order of a few percent, which is typical for XPCS

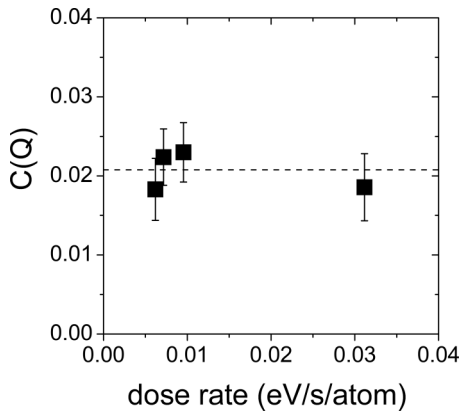

FIG. 2. The contrast $\mathcal{C}(Q_{max})$ obtained for a $(Li_2O)_{0.14}$ $(B_2O_3)_{0.86}$ glass (squares) as a function of the x-ray dose rate, together with its average value (dashed line).

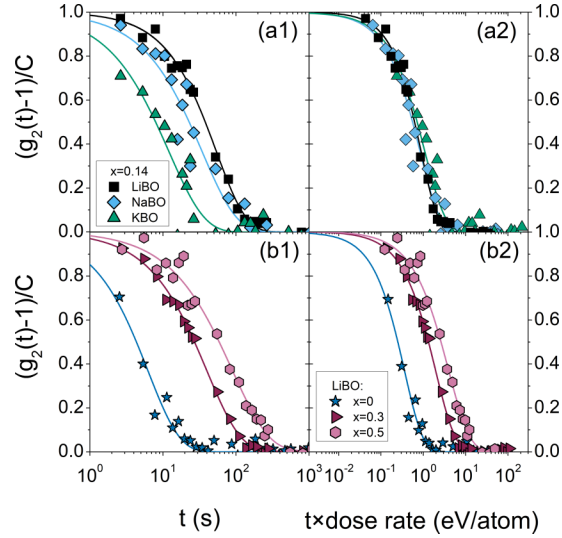

FIG. 3. Normalized intensity correlation functions (symbols) measured at room temperature (300 K) and at the position, Q_{max}, of the structure factor maximum in (a1): $(M_2O)_{0.14}(B_2O_3)_{0.86}$, where M = Li (black squares, LiBO), Na (light-blue diamond, NaBO), and K (green triangles, KBO); and (b1): $(Li_2O)_x(B_2O_3)_{1-x}$, with $x = 0$ (pure B_2O_3, blue stars), $x = 0.30$ (dark-violet triangles), and $x = 0.50$ (magenta hexagons). The data in (a1) have been collected with an incident beam flux $F = 1.7 \times 10^{10}$ ph/s and an exposure time per image $\Delta t_e = 0.4$ s. The data in (b1) have been collected with $F = 3.2 \times 10^{10}$ ph/s and $\Delta t_e = 0.8$ s for pure B_2O_3 while with $F = 3.9 \times 10^{10}$ ph/s and $\Delta t_e = 0.6$ s for the other two glasses. (a2) and (b2) Same data as in (a1) and (b1), respectively, with the time axis multiplied by the dose rate per atom. The measured functions are reported together with the best fitting stretched exponentials [Eq. (2)].

experiments in wide angle configuration and due to the limited longitudinal coherence of the beam [2].

III. RESULTS AND DISCUSSION

Figure 3(a1) shows a series of $g_2(Q_{max}, t)$ functions measured in vitreous $(M_2O)_x(B_2O_3)_{1-x}$ with M = Li, Na, and K and $x = 0.14$, all collected with a comparable average x-ray beam flux, $\langle F \rangle$. Given that the thicknesses of the different samples are similar (see Table I), Fig. 3(a1) suggests that the characteristic time, $\tau(Q_{max})$, depends on the absorbed x-ray flux, $\langle F \rangle_{abs}$, rather than on the incident x-ray flux, $\langle F \rangle$, in agreement with previous observations [10,11]. $\tau(Q_{max})$ seems in fact controlled by x-ray absorption and thus by the atomic number of the alkali modifier: the heavier the alkaline atom, the faster the relaxation time. The shape parameters, $\beta(Q)$, extracted from the KWW fits for a given glass do not show any significant dependence on the dose rate [see Fig. 4(a)]. This result confirms previous studies of the x-ray beam induced dynamics in oxide glasses [9–12]. The corresponding values averaged over the curves measured with different x-ray dose rates are reported in Fig. 4(b) as a function of the molar fraction x for all samples studied here. In all cases, the obtained values of $\beta(Q)$ correspond to a stretched exponential decay ($\beta \leqslant 1$). A similar stretched exponential behavior has been reported in Ref. [29] for a sodium silicate glass, in Ref. [10]

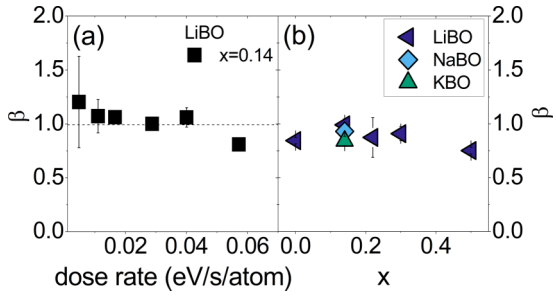

FIG. 4. (a) The shape parameter $\beta(Q_{\max})$ for a $(Li_2O)_{0.14}(B_2O_3)_{0.86}$ glass (squares) as a function of the dose rate, together with the average value (dashed line). (b) $\beta(Q_{\max})$, averaged over the measurements carried out at different x-ray dose rates, as a function of the alkali molar fraction, x. Different symbols refer to different glasses as reported in the legend.

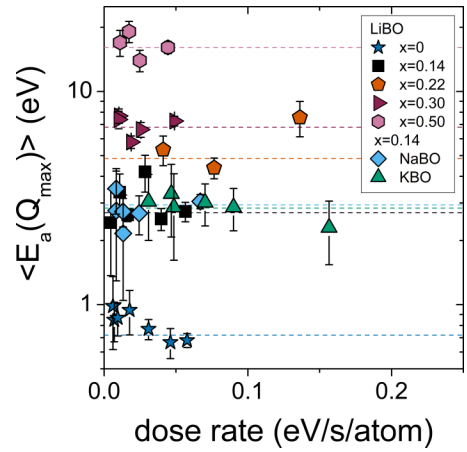

FIG. 5. Average energy absorbed per atom, $\langle E_a(Q_{\max})\rangle$, that induces an atomic displacement over at least an interatomic distance as a function of dose rate. Different symbols refer to different samples as reported in the legend. The mean values of $\langle E_a(Q_{\max})\rangle$ for each sample are indicated as horizontal lines.

for a boron oxide glass, in Ref. [12] for a lithium borate glass, and in Ref. [11] for a series of Rb and Cs borate glasses; a compressed exponential decay ($\beta > 1$) has instead been observed in Ref. [9] in the case of silicon and germanium oxide glasses. The reasons behind these qualitative differences between different glasses are not yet clear.

It is also worth observing that the values for β reported in Fig. 4(b) are somewhat higher than those reported in Ref. [11] for a series of Cs and Rb borate glasses, and that the decreasing trend of β with x in the $0 \leqslant x \leqslant 0.3$ range reported there is not observed in the present data. This might of course be due to intrinsic differences between Li, Cs, and Rb borate glasses.

The decay time, $\tau(Q)$, of the autocorrelation functions $g_2(Q,t)$ measured in oxide glasses seems controlled by the x-ray dose rate via a material-dependent coefficient [10,12]. This coefficient can be expressed in terms of the average energy, $\langle E_a(Q)\rangle$, absorbed per atom in the decay time τ:

$$\langle E_a(Q)\rangle = \frac{e}{e-1}\frac{E_{\rm ph}\langle F\rangle_{\rm abs}\langle\tau(Q)\rangle}{N_{\rm tot}}. \qquad (3)$$

Here, $\langle\tau(Q)\rangle = \tau(Q)\Gamma[1/\beta(Q)]/\beta(Q)$ is the mean relaxation time [28]. The mean relaxation time is here used in place of the relaxation time [10] in order to get a value robust against uncertainties in the shape of the correlation function obtained from the fits. The obtained values of $\langle E_a(Q_{\max})\rangle$ are also reported in Table I, together with the parameters used to obtain $\langle E_a(Q_{\max})\rangle$ from $\tau(Q_{\max})$. As per Eq. (3), $\langle E_a(Q_{\max})\rangle$ is the average energy absorbed per atom and required to move it by $1/Q_{\max}$ or more. It is therefore a measure of the radiation hardness of the glass and a phenomenological parameter material dependent but independent of the x-ray dose rate.

It is now possible to show that the coefficient $\langle E_a(Q_{\max})\rangle$ depends on the glass via its structure. To demonstrate this, in Fig. 3(a2) the correlation functions of Fig. 3(a1) are reported as a function of the time multiplied by the dose rate per atom. This amounts to getting rid of the dependence of the decay time on the x-ray dose rate, as suggested by Eq. (3). The almost perfect overlap of the three curves in Fig. 3(a2) clearly demonstrates that, in the case of glasses with the same structure, $\langle E_a(Q_{\max})\rangle$ is the same: the chemical composition does not matter. Moreover, in Fig. 3(b1) the normalized intensity autocorrelation functions measured with a comparable dose rate are reported for lithium borate glasses with different metal oxide molar fractions and, thus, different structures. In this case, as shown in Fig. 3(b2), rescaling the time axis by the inverse dose rate per atom does not lead to an overlap of the curves. This confirms that the coefficient, $\langle E_a(Q_{\max})\rangle$, ruling the proportionality of the decay time on the inverse of the dose rate, depends on the structure.

More quantitative information can be gained fitting Eq. (2) to the experimental curves measured for the different samples and different dose rates. The most important parameter that can be extracted from the fits is $\langle E_a(Q_{\max})\rangle$. The values of $\langle E_a(Q_{\max})\rangle$ derived from Eq. (3) and the fitting parameters (see Table I) are reported in Fig. 5 as a function of the dose rate.

$\langle E_a(Q_{\max})\rangle$, for any given glass, is found to be (i) independent of the dose rate, consistently with Eq. (3); (ii) dependent only on the glass structure, consistently with what is shown in Fig. 3. Glasses with different structures show clearly different values of $\langle E_a(Q_{\max})\rangle$. More precisely, $\langle E_a(Q_{\max})\rangle$ depends monotonically on the metal oxide molar ratio: as x increases the average energy $\langle E_a(Q_{\max})\rangle$ quickly increases, as shown in Fig. 6. This rules out the ideas that (i) the glass transition temperature, T_g, fixes the timescale of the x-ray induced dynamics, as proposed in Ref. [11]. T_g is in fact a nonmonotonic function of x in the here explored x range [30]. (ii) The induced dynamics is faster ($\langle E_a(Q_{\max})\rangle$ smaller) for larger x as a consequence of the dynamics of the alkalis being faster, as inferred in a recent study of Cs and Rb borate glasses [11]. The argument of an increasing scattering weight for the alkali ions on increasing x clearly does not hold for the Li borate glasses studied here.

It is also interesting to observe that $\langle E_a(Q_{\max})\rangle$ ranges between a fraction of eV and few tens of eV, and is a measure of the radiation hardness of the glass. It seems then interesting to explore the relation between this parameter and the connectivity of the glass network.

A way to approach the problem of network connectivity in alkali borate glasses is within the so-called topological con-

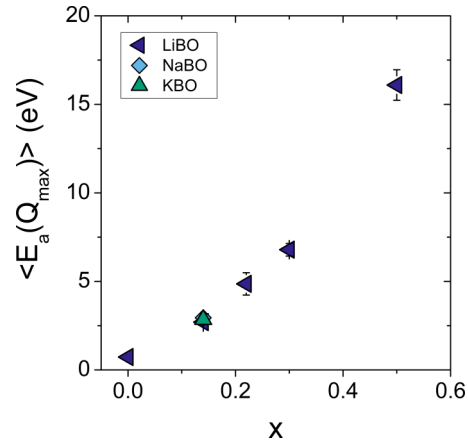

FIG. 6. Average energy absorbed per atom, $\langle E_a(Q_{\max})\rangle$, that induces an atomic displacement over at least an interatomic distance as a function of the alkali-metal oxide molar ratio, x. Different symbols refer to samples with different alkalis as reported in the legend.

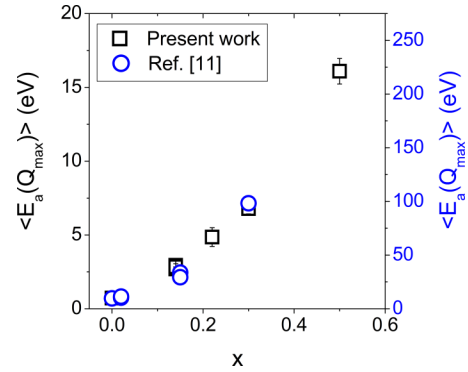

FIG. 8. Average energy absorbed per atom, $\langle E_a(Q_{\max})\rangle$, that induces an atomic displacement over at least an interatomic distance as a function of the alkali-metal oxide molar ratio, x. Black squares: data from the present work; blue circles: data from Ref. [11]. Each point corresponds to a different sample.

straint model. This model is based on the idea that the glass can be treated as a network of mechanical constraints [31,32]. The important ingredient here is the average number, n_c, of constraints per atom: the network can be floppy, isostatic, or stressed rigid depending on whether n_c is smaller, equal to, or larger than 3 (the network dimensionality). For what concerns alkali borate glasses, calculating n_c is not a trivial task due to the complex structural changes taking place on addition of alkali oxide. However, values of n_c as a function of the alkali-metal oxide molar ratio have been reported that allow describing trends in important properties such as T_g [30,33], the fragility [33], and the microhardness [34]. The values for $\langle E_a(Q_{\max})\rangle$ are reported as a function of n_c in Fig. 7 and show a monotonic dependence up to $x = 0.3$ ($n_c = 3.23$). This seems reasonable, since an increase of n_c corresponds to an increase in the energy density in the stressed-rigid network, as n_c counts the average number of constraints per atom. Interestingly, the borate glass with $x = 0.5$ stands at odds

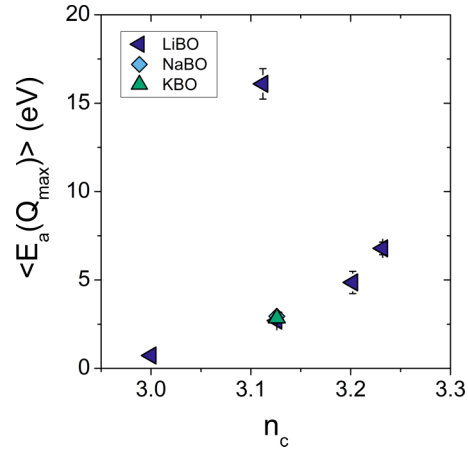

FIG. 7. Average energy absorbed per atom, $\langle E_a(Q_{\max})\rangle$, that induces an atomic displacement over at least an interatomic distance as a function of the average number of constraints per atom. Each point corresponds to a different sample.

with this simple correlation. This might be due to the fact that this correlation just does not hold for more complex glasses as $(Li_2O)_{0.5}(B_2O_3)_{0.5}$, where n_c might not be sufficient to capture the glass connectivity. For the case of Li borate glasses with values of $x > 0.3$, this is possibly due to the contribution to the network connectivity of clusters of Li ions [35], an effect that is not straightforward to map in terms of constraints.

Finally, we want to compare our results with those reported recently for a series of Rb and Cs borate glasses [11]. That experiment has been carried out using an incident energy of 13 keV at the beamline P10 of Petra III. The results of that experiment have been reported in terms of the characteristic decay time, $\tau(Q_{\max})$, for a given x-ray dose rate (1 eV per atom and per second) [11]. It is then possible to calculate the corresponding $\langle E_a(Q_{\max})\rangle$ values using those data. The values calculated using the data of Ref. [11] are reported in Fig. 8 (right y axis) together with those obtained here (left y axis). The two sets of data clearly do not overlap, in contradiction with Eq. (3). However, interestingly, they seem just related by a multiplicative factor.

The analysis proposed here in terms of $\langle E_a(Q_{\max})\rangle$ is delicate when one compares different experiments since it relies on the absolute measurement of the incident x-ray flux. The x-ray flux reported in Ref. [11] is 1×10^{11} photons/s with 100 mA of current in the storage ring. We suspect that this number might be overestimated. Recent measurements carried out at the same beamline and same energy (13 keV) show that the incident x-ray flux at that energy is rather close to 1.6×10^{10} photons/s. The data reported in Ref. [11] match, however, the ones that are here reported only when reduced by a factor of $\simeq$14 (the ratio of the maximum of the right to the left y scale; see Fig. 7), i.e., a factor that cannot be explained by our measurement of the beam flux at 13 keV. This might be a hint that the parameter $\langle E_a(Q_{\max})\rangle$ depends on the energy of the x-ray beam, a result that seems not obvious to explain at first sight. The energy dependence of $\langle E_a(Q_{\max})\rangle$ will have to be studied, however, in more detail before drawing definite conclusions.

IV. CONCLUSIONS

In conclusion, the recently discovered x-ray induced dynamics [9] has been characterized in some detail carrying out a systematic XPCS study on a series of alkali borate glasses. This effect is here described in terms of the average energy absorbed per atom, $\langle E_a(Q_{\max})\rangle$, that induces an atomic displacement over at least an interatomic distance. $\langle E_a(Q_{\max})\rangle$ is here shown to depend only on the glass structure and to be independent of the alkali species. More specifically, $\langle E_a(Q_{\max})\rangle$ is sensitive to the connectivity of the glass network.

This work offers then a scheme to rationalize the effects of the interaction of x rays with alkali borate glasses in the complex case where x rays cannot be considered any longer a small perturbation of matter (though they are still not permanently modifying its structure). This regime is becoming of greater and greater interest in modern x-ray-based experiments due to the continuous increase in brilliance of x-ray sources [36,37].

ACKNOWLEDGMENTS

We thank C. Armellini and F. Rossi for help in the preparation of the samples. Parts of this research were carried out at beamline P10 (experiments I-20150305 EC and I-20150425 EC) at DESY, a member of the Helmholtz Association (HGF). The research leading to this result has been supported by the project CALIPSOplus under the Grant Agreement No. 730872 from the EU Framework Program for Research and Innovation Horizon 2020.

[1] J. Als-Nielsen and D. McMorrow, *Elements of Modern X-Ray Physics* (Wiley, New York, 2011).
[2] G. Grübel, A. Madsen, and A. Robert, *Soft Matter Characterization* (Springer Netherlands, Dordrecht, 2008), p. 953.
[3] B. J. Berne and R. Pecora, *Dynamic Light Scattering: With Applications to Chemistry, Biology, and Physics* (Wiley-Interscience, New York, 1976).
[4] M. Sutton, S. G. J. Mochrie, T. Greytak, S. E. Nagler, L. E. Berman, G. A. Held, and G. B. Stephenson, Nature (London) **352**, 608 (1991).
[5] G. B. Stephenson, A. Robert, and G. Grübel, Nat. Mater. **8**, 702 (2009).
[6] M. Leitner, B. Sepiol, L.-M. Stadler, B. Pfau, and G. Vogl, Nat. Mater. **8**, 717 (2009).
[7] M. Fuchs, M. Trigo, J. Chen, S. Ghimire, S. Shwartz, M. Kozina, M. Jiang, T. Henighan, C. Bray, G. Ndabashimiye, P. H. Bucksbaum, Y. Feng, S. Herrmann, G. A. Carini, J. Pines, P. Hart, C. Kenney, S. Guillet, S. Boutet, G. J. Williams *et al.*, Nat. Phys. **11**, 964 (2015).
[8] N. Berrah, A. Sanchez-Gonzalez, Z. Jurek, R. Obaid, H. Xiong, R. J. Squibb, T. Osipov, A. Lutman, L. Fang, T. Barillot, J. D. Bozek, J. Cryan, T. J. A. Wolf, D. Rolles, R. Coffee, K. Schnorr, S. Augustin, H. Fukuzawa, K. Motomura, N. Niebuhr *et al.*, Nat. Phys. **15**, 1279 (2019).
[9] B. Ruta, F. Zontone, Y. Chushkin, G. Baldi, G. Pintori, G. Monaco, B. Rufflé, and W. Kob, Sci. Rep. **7**, 3962 (2017).
[10] G. Pintori, G. Baldi, B. Ruta, and G. Monaco, Phys. Rev. B **99**, 224206 (2019).
[11] K. Holzweber, C. Tietz, T. M. Fritz, B. Sepiol, and M. Leitner, Phys. Rev. B **100**, 214305 (2019).
[12] F. Dallari, G. Pintori, G. Baldi, A. Martinelli, B. Ruta, M. Sprung, and G. Monaco, Condens. Matter Phys. **22**, 43606 (2019).
[13] A. Martinelli, G. Baldi, F. Dallari, B. Rufflé, F. Zontone, and G. Monaco, Philos. Mag. **100**, 2636 (2020).
[14] D. L. Griscom, J. Non-Cryst. Solids **73**, 51 (1985).
[15] L. W. Hobbs, F. W. Clinard, S. J. Zinkle, and R. C. Ewing, J. Nucl. Mater. **216**, 291 (1994).
[16] J. Krogh-Moe, J. Non-Cryst. Solids **1**, 269 (1969).
[17] R. E. Youngman and J. W. Zwanziger, J. Phys. Chem. **100**, 16720 (1996).
[18] S. K. Lee, P. J. Eng, H. Mao, Y. Meng, M. Newville, M. Y. Hu, and J. Shu, Nat. Mater. **4**, 851 (2005).
[19] G. Ferlat, A. P. Seitsonen, M. Lazzeri, and F. Mauri, Nat. Mater. **11**, 925 (2012).
[20] J. Zhong and P. J. Bray, J. Non-Cryst. Solids **111**, 67 (1989).
[21] M. Bengisu, J. Mater. Sci. **51**, 2199 (2016).
[22] J. E. Shelby, J. Am. Ceram. Soc. **66**, 225 (1983).
[23] L. Shartsis, W. Capps, and S. Spinner, J. Am. Ceram. Soc. **36**, 35 (1953).
[24] Y. Ohta, M. Shimada, and M. Koizumi, J. Am. Ceram. Soc. **65**, 572 (1982).
[25] P10 Coherence Applications Beamline, http://photon-science.desy.de/facilities/petra_iii/beamlines/p10_coherence_applications/index_eng.html.
[26] D. Lumma, L. B. Lurio, S. G. J. Mochrie, and M. Sutton, Rev. Sci. Instrum. **71**, 3274 (2000).
[27] Y. Chushkin, C. Caronna, and A. Madsen, J. Appl. Cryst. **45**, 807 (2012).
[28] G. Williams and D. C. Watts, Trans. Faraday Soc. **66**, 80 (1970).
[29] B. Ruta, G. Baldi, Y. Chushkin, B. Rufflé, L. Cristofolini, A. Fontana, M. Zanatta, and F. Nazzani, Nat. Commun. **5**, 3939 (2014).
[30] W. Takeda, C. J. Wilkinson, S. A. Feller, and J. C. Mauro, J. Non-Cryst. Solids X **3**, 100028 (2019).
[31] J. C. Phillips, J. Non-Cryst. Solids **34**, 153 (1979).
[32] M. F. Thorpe, J. Non-Cryst. Solids **57**, 355 (1983).
[33] J. C. Mauro, P. K. Gupta, and R. J. Loucks, J. Chem. Phys. **130**, 234503 (2009).
[34] M. M. Smedskjaer, J. C. Mauro, and Y. Yue, Phys. Rev. Lett. **105**, 115503 (2010).
[35] E. Cristos-Platon Varsamis, A. Vegiri, and E. I. Kamitsos, Phys. Rev. B **65**, 104203 (2002).
[36] M. Eriksson, J. F. van der Veen, and C. Quitmann, J. Synchrotron. Radiat. **21**, 837 (2014).
[37] P. G. O'Shea and H. P. Freund, Science **292**, 1853 (2001).